Covariability of climate and streamflow in the Upper Rio Grande from interannual to interdecadal timescales

M. Pascolini-Campbell[a,*], Richard Seager[b], Ariane Pinson[c], Benjamin I. Cook[d,b]

[a] Department of Earth and Environmental Sciences, Columbia University, New York, NY, United States
[b] Lamont-Doherty Earth Observatory of Columbia University, Palisades, NY, United States
[c] United States Army Corps of Engineers, Albuquerque District, Albuquerque, NM, USA
[d] NASA Goddard Institute for Space Studies, New York, USA

ABSTRACT

Study region: The Upper Rio Grande (URG) flows from its headwaters in Colorado, U.S., and provides an important source of water to millions of people in the U.S. states of Colorado, New Mexico, Texas, and also Mexico.

Study focus: We reassess the explanatory power of the relationship of sea surface temperatures (SST) on URG streamflow variability on interannual to interdecadal timescales. We find a significant amount of the variance of spring-summer URG streamflow cannot be fully explained by SST.
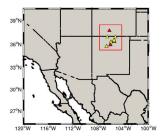
New hydrological insights: We find that the interdecadal teleconnection between SST and streamflow is more clear than on interannual timescales. The highest ranked years tend to be clustered during positive phases of the Pacific Decadal Oscillation (PDO). During the periods of decadal high flow (1900–1920, and 1979–1995), Pacific SST resembles a positive PDO pattern and the Atlantic a negative Atlantic Multidecadal Oscillation (AMO) pattern; an interbasin pattern shown in prior studies to be conducive to high precipitation and streamflow. To account for the part of streamflow variance not explained by SST, we analyze atmospheric Reanalysis data for the months preceding the highest spring-summer streamflow events. A variety of atmospheric configurations are found to precede the highest flow years through anomalous moisture convergence. This lack of consistency suggests that, on interannual timescales, weather and not climate can dominate the generation of high streamflow events.

1. Introduction

At 3051 km in length, and with a drainage area of approximately 472,000 km², the Rio Grande is the fourth longest river in North America. It provides water to 5 million people for agricultural, municipal and industrial purposes in the U.S. states of Colorado, New Mexico, and Texas, and in Mexico (Woodhouse et al., 2012) (Fig. 1). The majority of the flow in the river above its confluence with the Rio Conchos near Presidio, Texas, originates as snowmelt runoff from the mountains in southeastern Colorado and northern New Mexico (Lee et al., 2004; Khedun et al., 2010; Woodhouse et al., 2012) (collectively, the Upper Rio Grande (URG), with a drainage area of approximately 43,000 km² (Lee et al., 2004)). Sixty to sixty-five percent of inflows originate in the headwaters region, consisting of the southern Rocky Mountains and San Luis Valley of southwestern Colorado; flows along the Rio Chama and the Jemez River collectively account for another 25 percent of native inflows to the URG, with the remaining inflows coming from minor
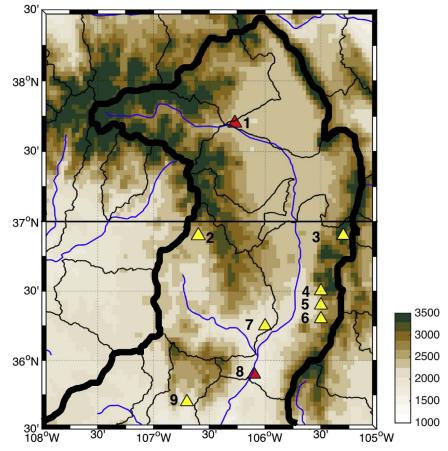
Fig. 1. Map showing elevation (meters), delineation of upper Rio Grande basin (thick black line), and location of USGS stream gages used in this study: (1) Del Norte, (2) Rio Chama, (3) Santistaven creek, (4) Rio Hondo, (5) Rio Lucero, (6) Rio Pueblo de Taos near Taos, (7) Rio Ojo, (8) Otowi, (9) Jemez river. Red marker indicates stream gage is located on main stem, yellow marker indicates stream gage is located on a tributary. Inset above shows location of upper Rio Grande region.

tributaries (Llewellyn and Vaddey, 2013). The majority of the 5 million water users are located south of the Jemez River confluence in the Middle Rio Grande (from the Jemez River to the El Paso Valley). High interannual variability in streamflow poses significant challenges for water supply and flood risk management. Improved understanding of the climate controls on Rio Grande flow variability is essential to improve management of water resources.

Studies have shown that precipitation and streamflow in the Southwestern United States (SWUS) in general are affected by a range of diverse drivers, including the El Niño-Southern Oscillation (ENSO), the Pacific Decadal Oscillation (PDO) and the Atlantic Multidecadal Oscillation (AMO), as well as the North American Monsoon (NAM). However, the failure of recent El Niño events to generate correspondingly large spring runoff volumes suggests that these relationships are not straightforward. This paper reassesses the impacts of ENSO, PDO, and AMO on streamflow in the Rio Grande basin above Albuquerque, New Mexico, and shows that these teleconnections are an incomplete explanation of the variance in flows.

On interannual timescales, ENSO produces above normal precipitation and streamflow for the SWUS when it is in its warm phase (El Niño) (Kahya and Dracup, 1993, 1994). On interannual timescales El Niño has also been found to be associated with above-normal precipitation and streamflow anomalies in the URG basin (Lee et al., 2004; Khedun et al., 2010). The PDO has also been found to produce above normal northern hemisphere winter (December–January–February (DJF)) precipitation and streamflow during its positive phase (Barlow et al., 2001; Cayan et al., 1999; Khedun et al., 2010; Pascolini-Campbell et al., 2015; Guan et al., 2005). The cold (warm) AMO produces positive (negative) streamflow and precipitation anomalies in the SWUS (Enfield et al., 2001; Thomas, 2007; Nowak et al., 2012). This relationship is strengthened with a concurrent positive PDO phase (McCabe et al., 2004). The NAM

brings a northern hemisphere summer (July-August-September (JAS)) peak in rainfall (Adams and Comrie, 1997; Barlow et al., 1998) and NAM variability drives streamflow variability (Pascolini-Campbell et al., 2015). As this paper focuses on flows resulting from snowmelt runoff, the effects of the NAM on late summer flows is not considered further. ENSO, PDO and AMO have also been found to modulate streamflow in other river basins around the world (Ward et al., 2016; Córdoba-Machado et al., 2016; Kiem and Franks, 2004).

Streamflow predictability is also influenced by land surfaces processes via the interaction of precipitation, evapotranspiration, snowmelt, soil moisture and vegetation (Koster et al., 2010; Maurer and Lettenmaier, 2003). Infiltration into soils, evapotranspiration and canopy water storage can all contribute to reducing runoff of water to streams. Water storage in snowpack and its melt also will impact the timing and magnitude of water delivery to the rivers. Variability of these different processes will influence streamflow timing (Hamlet et al., 2007). Therefore, despite the observed teleconnection between precipitation and SST, the influence of SST on streamflow is modulated by a variety of complex land surface processes.

The purpose of this study is to re-evaluate the climatic drivers which produce the observed mean seasonal cycle of URG streamflow, and mean flow variability on interannual to decadal timescales. Second, we will investigate the drivers of the highest mean monthly northern hemisphere spring-summer (April to September) streamflow anomalies. This study extends previous research on the URG through consideration of the combined role of the Pacific and Atlantic, a longer period of study extending from 1920 to 2016, interannual and decadal variability, and both mean flow and high flow variability. In addition, sea surface temperatures do not account for all streamflow variability. Therefore, the present study will also consider the atmospheric configurations that correspond to streamflow anomalies that can occur across a range of SST states.

Using URG stream gage data, observed precipitation, observed sea surface temperature and atmospheric Reanalysis, this study aims to provide a more complete understanding of URG streamflow variability over the past several decades. The following questions are investigated:

- What climatic drivers produce the observed seasonal cycle of URG flow?
- Which configurations of Pacific and Atlantic SST drive flow variability on timescales of years to decades for the URG and how strong are these relations?

This investigation will advance understanding of the climatic drivers of URG flow variability, and of extreme high and low flows to the benefit of water management activities. In particular, it will be shown that prior work has overstated the role of sea surface temperature anomalies in driving URG flow variability.

2. Data and methods

To analyze the natural drivers of Rio Grande streamflow at its headwaters, we use seven United States Geological Survey gages (USGS) on tributaries in New Mexico (Fig. 1). Tributaries are selected because all stream gages on the Rio Grande main stem are affected by regulation and water withdrawals. Instead, we analyze data from the following unmodified New Mexico tributaries (arranged from northernmost to southernmost): Rio Chama near La Puente (USGS 08284100), Santistevan Creek near Costilla (USGS 08253500), Rio Hondo near Valdez (USGS 08267500), Rio Lucero near Arroyo Seco (USGS 08271000), Rio Pueblo de Taos near Taos (USGS 08269000), Rio Ojo Caliente near Madera (USGS 08289000) and Jemez River near Jemez (USGS 08324000). We use mean monthly streamflow data for these sites to examine flow. We compare the streamflows of these rivers to the naturalized flow record for two gages lying on the main Rio Grande stem itself (Rio Grande near Del Norte, CO, (USGS 08220000), and Rio Grande at Otowi Bridge, New Mexico, (USGS 08313000)) (time period available shown in Table 1). These gages are located in the upper reaches of the Rio Grande in an area characterized by mountainous terrain with peaks exceeding 3500 m. These stream gages drain areas as small as 6 km^2(Santistaven) up to 37,036 km^2 (Otowi) (compared to a drainage area of 43,000 km^2 for the URG (Lee et al., 2004)). We find high correlation (ranging from $r = 0.69$ to $r = 0.84$ with Del Norte, and $r = 0.79$ to $r = 0.92$ for Otowi) between the Rio Grande gages and the tributary flows, thus allowing the tributaries to serve as suitable indicators of the natural flow variability (Table 1, last column).

Table 1
Summary of USGS station data.

Gage name	Gage number	Temporal availability (Monthly statistics)	Drainage area (sq km)	Elevation (m above NGVD29)	Correlation: Del Norte (Otowi) (r-value)
Del Norte	08220000	1908–2015	3419	2432	1.00 (0.84)
Rio Chama	08284100	1955–2014	1243	2158	0.84 (0.92)
Santistaven	08253500	1937–2014	6	2901	0.75 (0.79)
Hondo	08267500	1934–2015	94	2331	0.69 (0.86)
Lucero	08271000	1913–2014	43	2453	0.72 (0.84)
Pueblo	08269000	1913–2014	173	2249	0.69 (0.87)
Ojo	08289000	1932–2016	1085	1937	0.75 (0.91)
Otowi	08313000	1919–2016	37036	1672	0.84 (1.00)
Jemez	08324000	1936–2016	1217	1713	0.71 (0.81)

Table 2
Summary of SNOTEL station data.

Station name	Station number	Temporal availability (monthly statistics)	Elevation (m)
Upper Rio Grande	839	1986–2015	2865
Red River Pass #2	715	1978–2015	3002
Palo	1170	2010–2015	2849
Elk Cabin	921	1996–2015	2502

Seasons discussed in the paper refer to the northern hemisphere. The area receives precipitation as snow during winter months, which melts in the spring and summer. Rainfall is greatest in the summer months when the area is affected by local-scale convective activity. Analysis will cover the period of the full flow records (see Table 1). We use Pearson's correlation throughout to assess the strength of the relationships between variables. Given the positive-skew of streamflow, we use the log-value of streamflow when carrying out the correlations between streamflow.

The precipitation dataset we use is from the Parameter Regression on Independent Slopes Model (PRISM; in units of mm/month on a 4 km grid), which uses a well-verified, terrain-sensitive algorithm to interpolate between available stations over the period 1895-present (Daly et al., 2008). We average precipitation over the catchment area of each of the stream gages to investigate local variability. We acknowledge the limitations of using gridded precipitation data, which has been found to underestimate extremely high rainfall events, which could implicate our understanding of high monthly streamflow events (King et al., 2013). Gridded precipitation data is also less reliable at higher elevations, which is an additional caveat given the high altitude of the drainage gages used in this study (see Table 1) (Tozer et al., 2012). SNOTEL data is used for snow water equivalence (SWE) from sites lying in proximity to the stream gages used (information in Table 2). We use four different SNOTEL sites which corresponds to the location of gages used: Upper Rio Grande (corresponding to Del Norte, Rio Chama and Santistaven), Red River Pass 2 (Hondo, Lucero and Pueblo), and the average of Palo and Elk Cabin (Ojo, Otowi and Jemez). For SST, we use ERSST V4 reanalysis data (in units of degrees Celsius on a $2° \times 2°$ global grid) (Smith et al., 2008). We use ERA Interim data for vertically integrated moisture flux (mean and transient) to analyze the atmospheric moisture delivery patterns ($1.5° \times 1.5°$ global grid) (1979–2014) (Dee et al., 2011). We also use ERA Interim precipitation data for comparison to the moisture flux.

We use the following SST indices created from ERSST V4: NINO3.4 (SST in the Pacific area-averaged over 5S–5N, and 170W–120W), Pacific Decadal Oscillation (PDO) index (the leading principal component of monthly SST anomalies in the North Pacific Ocean north of 20N) (Zhang et al., 1997), and the Tropical North Atlantic (TNA) index (average anomaly of monthly SST averaged over 5.5N to 23.5N and 15W to 57.5W) to represent AMO (Enfield et al., 2001). We use the TNA due to its high correlation with the AMO, and also due to the fact Atlantic impacts on SWUS climate originate largely from the tropics (Kushnir et al., 2010).

3. Results

3.1. Climatology and variability of URG streamflow, precipitation and temperature

The water year (October–September) mean streamflow for the tributaries Rio Chama, Santistaven, Hondo, Lucero, Pueblo, Ojo and Jemez stream gages is highly correlated with those of Del Norte and Otowi on the main stem of the Rio Grande (Table 1, last column). The timing of the peak flow is also fairly consistent between the main stem and the tributaries, with highest flows occurring in April–May–June–July (AMJJ) (Fig. 2). Gages further north in the basin (Del Norte, Rio Chama, Santistaven, hereafter referred to as 'northern gages') have peak flows occurring more in May-June-July, whereas gages more south in the basin (Ojo, Otowi and Jemez, hereafter 'southern gages') have peak flows occuring earlier in April-May-June. Middle gages (Hondo, Lucero, Pueblo, hereafter 'middle gages') tend to peak in May-June. This is consistent with above-freezing temperatures and snowmelt occurring earlier further south in the basin, contributing to earlier spring-summer flows (see Fig. 3 below). The similar timing in streamflow is expected given the proximity of these stream gages, as well as their comparable elevations in the basin (Table 1). The hydrographs (Fig. 2) also illustrate the positive skew of the data: many of the highest flows exceed 1.5 times the interquartile range of the data (as demonstrated by the outliers denoted by a red cross).

We investigate the seasonal cycles of precipitation and SWE using PRISM data averaged over the drainage area of the stream gage and SNOTEL gages located at proximity to the gages respectively (Fig. 3). Precipitation over the northern gages displays a bimodal peak: the first occurring in February-March–April (reaching a maximum of 75 mm/month for Rio Chama), and the second in July–August–September (reaching a maximum of approximately 75 mm/month for Rio Chama, Santistaven and Lucero). The southern gages have a more pronounced summer precipitation maximum (June–July–August) indicative of the monsoon influence. For the northern gages, SWE peaks in March whereas for the southern gages the SWE peaks earlier in February. The earlier decline in SWE in the southern gages is mirrored in the earlier peak streamflow (Fig. 2).

Interannual variability in AMJJ streamflow is broadly synchronous among gages. Fig. 4 (top panel) shows the timeseries of both high pass and low pass AMJJ streamflow using a cut off frequency of seven years (see below for details of the filter). Similar timing in anomalously high annual flows is observed to occur between the different gages, such as the high flow peaks in 1985, 1995 and 2005. Magnitudes are far smaller for the tributaries which drain much smaller basins in the system such as Hondo, Lucero and Pueblo (see Table 1 for drainage area). The AMJJ timeseries in Fig. 4 also contain a similar pattern of low frequency high flow centered around
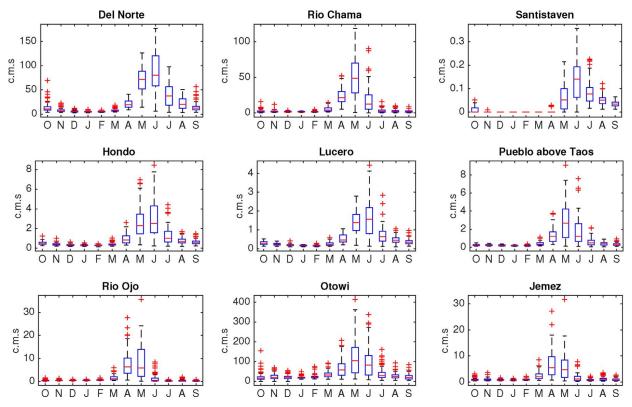
Fig. 2. Boxplots of monthly streamflow (c.m.s.) over length of record for each stream gage. For each boxplot, the central mark is the median, the edges of the box are the 25th and 75th percentiles, the whiskers extend to the most extreme data points not considered outliers, and outliers are plotted as crosses.
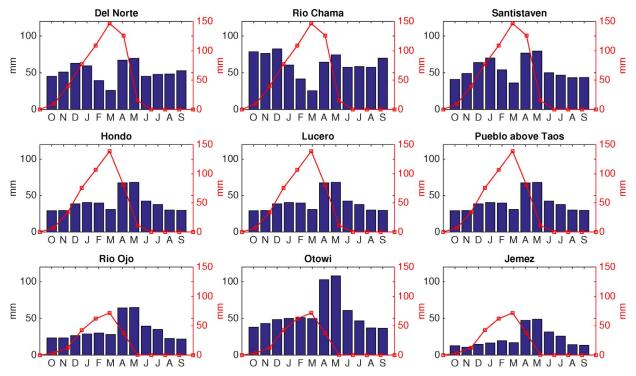

Fig. 3. Seasonal cycle of PRISM precipitation area averaged over each gage (bars) (mm/month) and snow water equivalent SNOTEL gage data (red lines) (mm/month).

1985 and declining flow from 1996 to present. In the longer streamflow timeseries (for Del Norte) this low frequency variability is seen to also produce above normal flow in the early century (1900–1920) and lower flow between 1945 and 1975. The PRISM timeseries of average annual water year precipitation in the contributing watershed above the stream gages for the period 1895 to
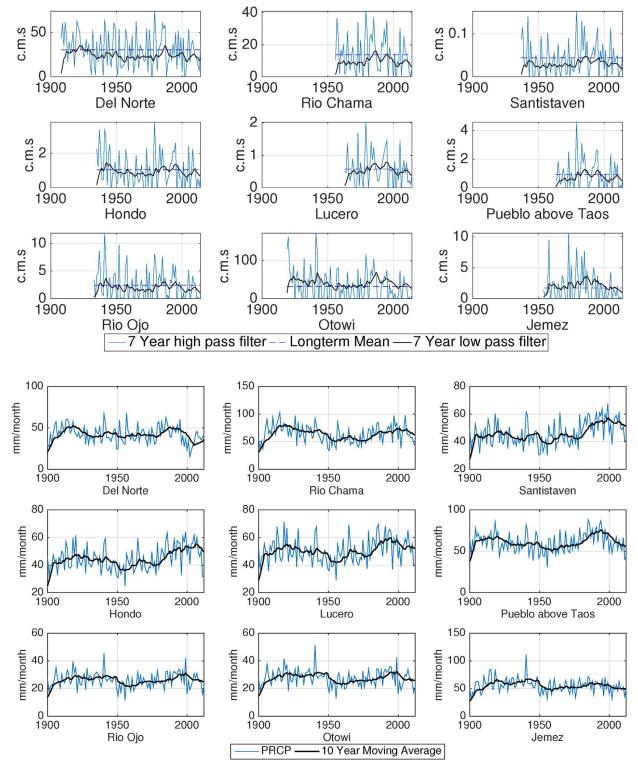
Fig. 4. Top: Streamflow timeseries for high pass (blue line) and low pass (black line) filtered AMJJ for each stream (c.m.s.) using a cutoff frequency of 7 years. Blue-dashed line is long term mean for high pass filtered throughstreamflow. Bottom: PRISM precipitation timeseries for annually averaged water year (October to September) (blue line) (mm/month) and 10 year moving average (black line) area-averaged over the catchment of each stream gage.

2014 (Fig. 4 (bottom graphs)) shows corresponding wetter than average conditions in the early 20th century (1900–1920) followed by a decline in the mid-century to drier than average conditions (from approximately 1945 to 1975). The precipitation decadal mean then increases again from the 1980s to around 2000 after which it again tends to decline.
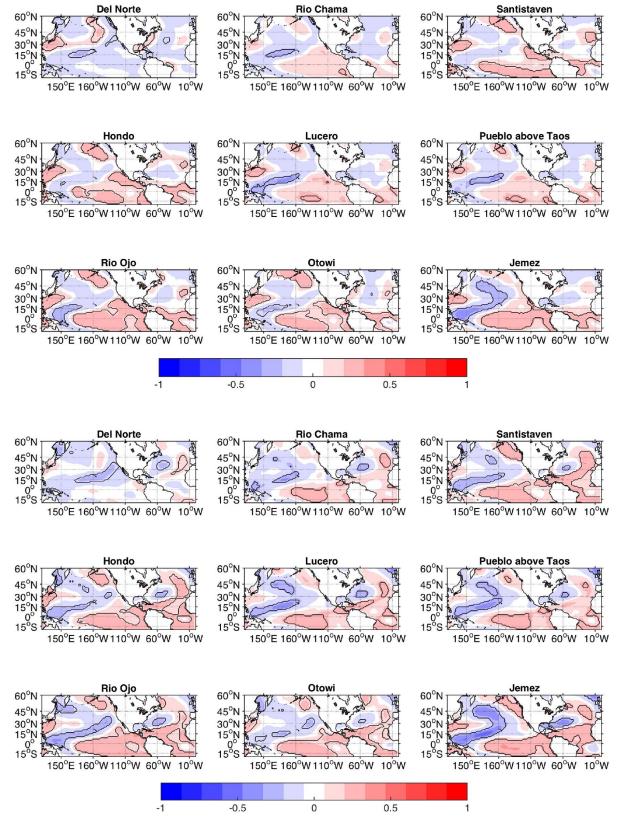
Fig. 5. High pass filtered ERSSTV4 DJF (top) and MAM (bottom) SST correlated with high pass filtered AMJJ streamflow for all years covered by stream gages. High pass filtering was done using a cutoff frequency of 7 years. Colorbar indicates magnitude of the correlation [*r* = 0 to 1]. Areas that are significant at *p* < 0.1 lie within the black contour.
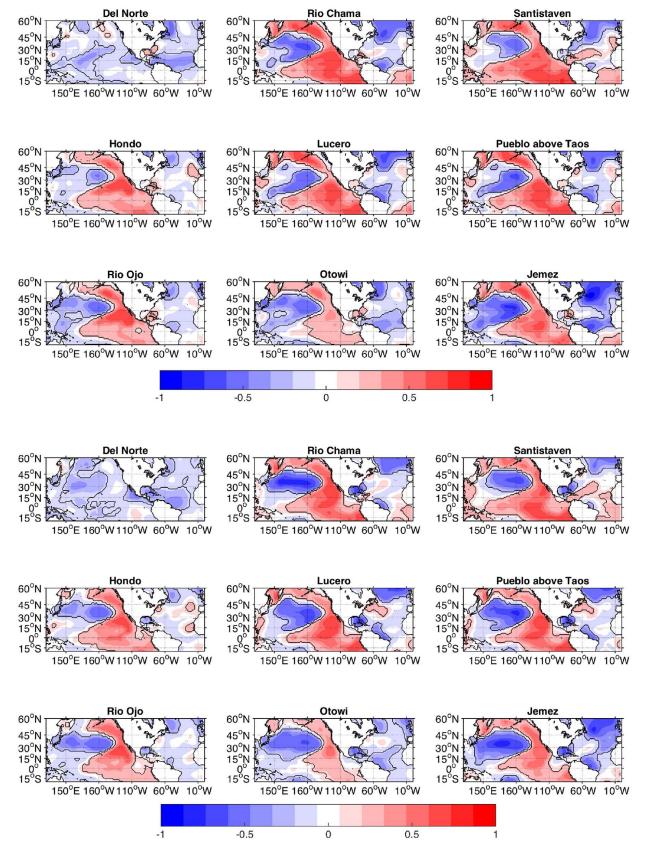
Fig. 6. Low pass filtered ERSSTV4 DJF (top) and MAM (bottom) SST correlated with low pass filtered AMJJ streamflow for all years covered by stream gage. Low pass filtering was done using a cutoff frequency of 7 years. Colorbar indicates magnitude of the correlation [r = 0 to 1]. Areas that are significant at $p < 0.1$ lie within the black contour.
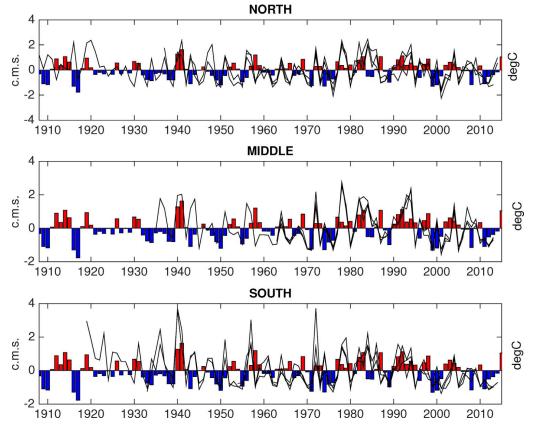
Fig. 7. Bar graph shows NINO3.4 SST anomaly (°C) for the DJF season, and black lines show the standardized anomaly for the maximum monthly flow occurring in each water year (c.m.s.). These are arranged as follows: the three most northern gages (Del Norte, Rio Chama, Santistaven) (top panel), middle gages (Hondo, Lucero, Pueblo) (middle panel) and southern gages (Ojo, Otowi, Jemez) (bottom panel).

3.2. Relation of peak flow variability to antecedent precipitation and ocean states

AMJJ streamflow is influenced by precipitation during the preceding fall to spring (October to May). Since the main Pacific SST teleconnection season is during the DJF and MAM seasons, for the rest of this section we focus on the season December to May. To understand how December to May precipitation influences streamflow, we analyze the relationship among key drivers of precipitation variability (ENSO, PDO, TNA) and streamflow in the URG using both high and low pass filtered streamflow and SST data (Figs. 5 and 6). The high (low) pass filter attenuates frequencies below (above) seven years to only capture high (low) frequency variability. We filter frequencies above and below seven years since this period approximately divides interannual ENSO from decadal PDO while the AMO only occurs on the longer timescale. ENSO variability occurs on a timescale of 3 to 7 years (Trenberth et al., 1998). We follow the methods of Zhang et al. (1997) who filtered SST using high and low pass filters with a cut off of 6 years to separate interannual from interdecadal variability. In our case, we select 7 years to represent the upper range of ENSO variability. We performed the analysis using cut off filters for different years (6, 7, 8, 10) and found there to be no significant difference in the results for the different cut off years for the low and high pass filters with slight alteration of the cut off period.

The filter we use is the Butterworth filter. We use effective sample size for significance testing in order to account for the issue of autocorrelation arising from the smoothed data series. We are aware of the potential limitations of assuming linearity between SST and streamflow as has been noted in prior work (Córdoba-Machado et al., 2016; Kiem et al., 2003). Hence, we performed composite analyses of SST corresponding to high and low streamflow years for each gage, and these confirmed a predominantly linear relationship between SST and AMJJ streamflow. We therefore have confidence in using the linear correlations between SST and streamflow to investigate this relationship.

In the high pass filtered correlations, AMJJ streamflow is weakly positively correlated with Pacific SSTs in both DJF and MAM (Fig. 5). The expected negative correlation between AMJJ streamflow and north Atlantic SST is not evident in either DJF or MAM. Furthermore, the correlations for high pass filtered data are for the most part not significant at $p < 0.10$ (denoted by the black contours). The correlations become significant in the tropical Pacific for gages further south in the basin.

Turning to the low pass filtered data (Fig. 6), correlations with SSTs are higher for this smoothed time series, with peak positive correlations between $r = 0.50$ to $r = 0.75$ in the eastern tropical Pacific and $r = -0.50$ to $r = -0.75$ in the subtropical Atlantic. This is unsurprising, since we expect the correlations to be stronger on decadal timescales due to the aggregated effect from multiple warm (cold) years in the tropical Pacific (Atlantic) on SWUS precipitation (Chen and Wallace, 2015; Cayan et al., 1999; Enfield et al., 2001; Thomas, 2007; Nowak et al., 2012). Despite the limited significance (our effective degrees of freedom dropped from $n = 36$ to $n = 8$
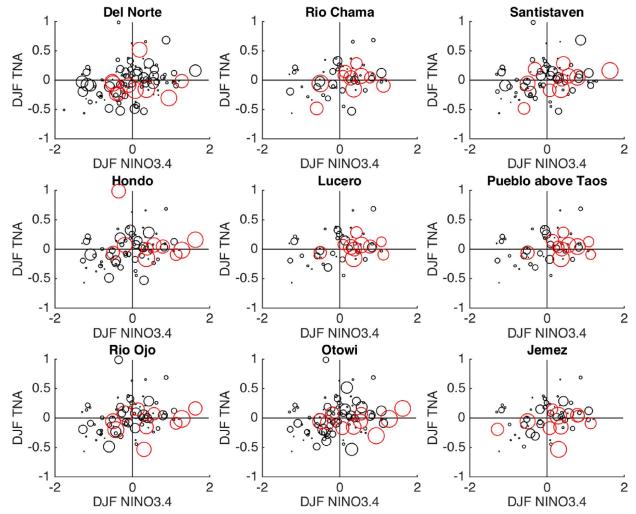
Fig. 8. Scatter plot of NINO3.4 DJF, TNA DJF and the associated AMJJ streamflow at each stream gage. The size of the AMJJ flow is exponentially scaled and represented by the radius of the circular marker. Units on the *x*- and *y*-axis °C. Red circle coloring indicates the event is a top 10 AMJJ streamflow in the period of record.

in the smoothed time series), these results are consistent with the expected physical processes (McCabe et al., 2004; Schubert, 2009). We find that the predictability is increased on decadal timescales.

To address further the interannual variability of Pacific SST and streamflow, we find the maximum monthly flow in a given water year and plot it along with the value of the DJF NINO3.4 index for the full length of each stream gage (Fig. 7, separately for the northern, middle and southern gages). The northern gages correspond less to NINO3.4 SST (maximum $r = 0.25$) than the middle and southern gages (maximum $r = 0.31$). This is consistent with the ENSO precipitation teleconnection pattern being stronger in the southern half of the URG region. Results indicate that although high flows typically correspond with positive DJF NINO3.4 values, several notable exceptions occur. This includes the highly positive flow anomalies in 1942,1984 and 1985 following negative DJF NINO3.4, and negative flow anomalies in 1958 and 2002 following a positive DJF NINO3.4.

Fig. 8 extends this analysis to include the influence of both the tropical Pacific and Atlantic on streamflow. We plot the AMJJ streamflow for each year going back the full length of each stream gage. The magnitude of AMJJ flow is scaled and plotted as marker diameter along with the corresponding value of DJF NINO3.4 and DJF TNA in the season preceding the high flow. The circle is colored red if it is one of the top 10 AMJJ flow events in the record. Positive DJF NINO3.4 and negative DJF TNA, based on prior work, is the configuration expected to produce above normal streamflow in the SWUS (McCabe et al., 2004; Schubert, 2009). Fig. 8 shows in general that moving south in the basin leads to higher monthly streamflow occurring after warm NINO3.4. There is more variability in the impact of DJF TNA on AMJJ streamflow for the highest seasonal events, with high streamflow events occurring following both warm and cold DJF TNA. This Figure demonstrates that exceptions to the 'ideal' conditions conducive to high flow exist: high monthly streamflows can occur following cold NINO3.4 or warm TNA events (or both). We also used bootstrap statistics, and resampled the AMJJ streamflow data 1000 times and stratified it according to SST phase, and found that the percentage of total streamflow in each quadrant is no more than that which is likely to occur by chance at $p < 0.10$. These results again indicate the limited explanatory power of SST on interannual flows.

Given the limited explanatory power of SST on streamflow we also looked at atmospheric moisture convergence corresponding to
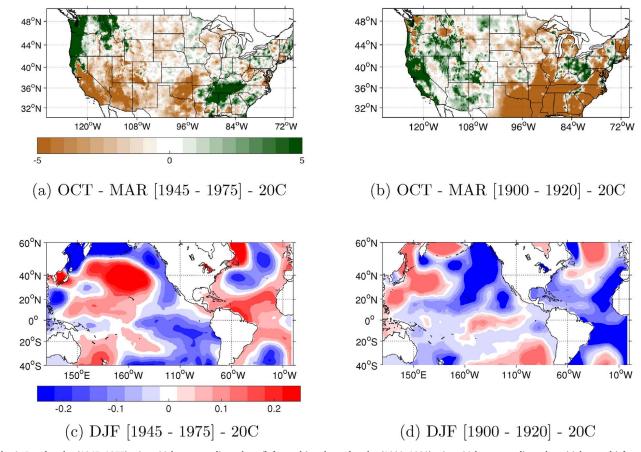
Fig. 9. Dry decades (1945–1975) minus 20th century climatology (left panels) and wet decades (1900–1920) minus 20th century climatology (right panels) for water year composite PRISM precipitation (top) and DJF ERSST V4 SST (bottom).

the highest streamflow events. Results indicated that a large variety of atmospheric circulation patterns can lead to wetting anomalies on the URG. The lack of a consistent pattern in atmospheric anomalies contributing to these high flow events suggests that many of them are forced by transient systems rather than SST.

3.3. Climatic causes of decadal variability of URG flow

To investigate the strength of the SST-streamflow relationship on decadal timescales we turn our analysis to the longer streamflow timeseries of Del Norte and Otowi (Fig. 4). In these streamflow timeseries we identify dry decades (1945–1975 and 1996–present) and wet decades (1900–1920 and 1979–1995). Fig. 9 contains composite anomalies for the early century dry decades (1945–1975) and wet decades (1900–1920) for both water year PRISM precipitation and DJF ERSST V4 SST. For the dry composite, widespread negative precipitation anomalies occur over the SWUS and include the region of the URG. The early wet composite has wet anomalies over the SWUS in a region more centered over the Rio Grande basin. This is the early 20th century North American pluvial of 1900 to 1917 (Woodhouse et al., 2005; Cook et al., 2011).

The pattern of DJF SST for the dry years indicate a region of cooling in the equatorial Pacific and along the North American west coast, positive anomalies in the central North Pacific and positive anomalies in the tropical North Atlantic (Fig. 9, bottom left panel). This decadal pattern of SST is consistent with the cool phase of the PDO (characterized by a cool equatorial Pacific and warm North Pacific (Zhang et al., 1997)), and the warm phase of the AMO (Enfield et al., 2001), ideal conditions for a drier than normal climate in the SWUS (Schubert, 2009). The composite for wet years indicates a warm equatorial Pacific, cool north east Pacific and cool tropical north Atlantic. The weakness of the tropical Pacific SST anomalies during the pluvials, however, is consistent with Cook et al. (2011) who found little evidence of tropical Pacific driving of the early 20th century pluvial. Again, this disconnect between the tropical Pacific and streamflow highlights the limited explanatory power of SST on streamflow.

Fig. 10 examines decadal variability for the later part of the twentieth century to present, for the two halves of the water year (October to March and April to September) in precipitation and SST. For October to March, the wet decades (1979–1995) minus the dry decades (1996–2015), show positive precipitation anomalies over the region of the URG, positive SST anomalies in the equatorial Pacific, negative SST in the north Pacific, and negative SST anomalies in the Atlantic. The Pacific SST pattern and the cyclonic flow over the central north Pacific are consistent with the positive phase of the PDO which has been associated with above normal streamflow and precipitation in the SWUS (Zhang et al., 1997; Barlow et al., 2001; Cayan et al., 1999; Pascolini-Campbell et al., 2015). The magnitude of these anomalies is reduced in April to September.
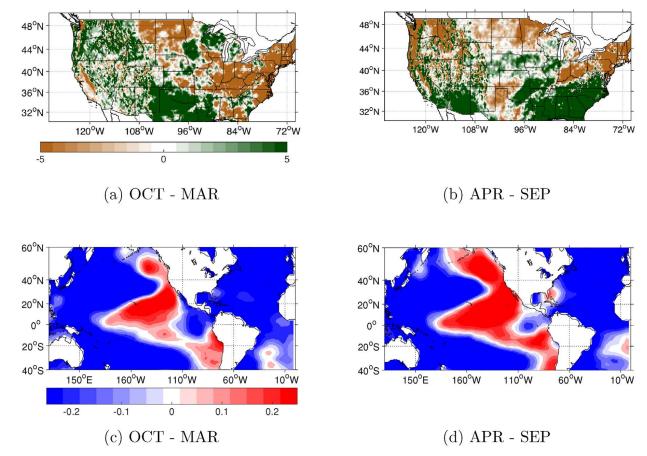
Fig. 10. Wet decades (1979–1995) minus dry decades (1996–2012) composites. Top panel: PRISM precipitation. Colorbar indicates magnitude of anomaly [mm/day]. Bottom panel: ERSSTV4 SST. Colorbar indicates magnitude of SST anomaly [°C]. October–March (left) and April–September (right).

4. Discussion and conclusions

This study has examined (1) the controls on the seasonal cycle and variability of URG streamflow, and (2) the ocean and atmosphere mechanisms which result in anomalous streamflow. We extend the work of previous authors on the role of ENSO and PDO on URG streamflow (Lee et al., 2004; Guan et al., 2005; Khedun et al., 2010; Kahya and Dracup, 1994), and other studies which examine the interrelationship of different modes of climate variability on SWUS precipitation (McCabe et al., 2004) by providing the following findings:

1. The mean seasonal cycle of streamflow for the URG is characterized by a spring-summer peak, which occurs later for northern gages and earlier for southern gages (Fig. 2). This is consistent with the timing of winter snowpack melt (Lee et al., 2004). Spring-summer streamflow is influenced the most by precipitation in the preceding winter-spring throughout the URG, with all months being about equally important.
2. Assuming a linear relationship between SST and AMJJ streamflow, as in prior studies of the URG (Lee et al., 2004; Khedun et al., 2010), the results suggest limited influence of the oceans on interannual flow variability. To the extent there is an influence, the ocean configuration favoring above normal URG streamflow consists of a warm equatorial Pacific and cold north Atlantic in the winter-spring preceding spring-summer flow (Trenberth et al., 1998; Enfield et al., 2001; McCabe et al., 2004; Kushnir et al., 2010). The relationship of flow to tropical SSTs weakens to the north, meaning that the areas producing the largest share of native inflow have the weakest relationship with tropical Pacific and Atlantic SSTs.
3. Some of the largest streamflow anomalies on interannual timescales do not follow the ideal conditions of a warm tropical Pacific and cold north Atlantic, such as 1942, 1984 and 1985. Analysis of atmospheric moisture transport for these years indicates that anomalous convergence located in the URG is driven by a variety of atmospheric circulation patterns. The lack of a consistent pattern in atmospheric anomalies contributing to these high flow events, suggests that many of them are forced by transient systems rather than persistent circulation anomalies driven by SST.
4. Decadal high flow periods from 1900–1920, 1979–1995, and low flow periods from 1945–1975 and 1996–2014, are found to be influenced by the phases of the PDO and AMO. The SST composite for dry decades (1945–1975) shows SST patterns characteristic of the cool PDO and warm AMO phases. The drop in URG streamflow in the most recent decades (1996–2014) is associated with a turn to a cool PDO and warm AMO. The increase in multiple warm Pacific SST years during positive PDO events was also found to produce above normal streamflow in studies of other basins (Kiem and Franks, 2004). We conclude that on decadal timescales,

sustained periods of both high and low flow can be explained in terms of oceanic decadal variability.

The ocean-atmosphere configurations described explain streamflow variability in the URG on timescales of months to decades. However, much of the streamflow variability on interannual timescales is still unexplained by the Pacific and Atlantic SST teleconnections. Several of the highest flow years do not follow a warm Pacific/cold Atlantic configuration. Further, atmospheric anomalies demonstrate a wide range of conditions which can produce localized URG wetting. This suggests there will be limited predictability of URG flow on interannual timescales. The aggregate effect of multiple warm Pacific SST years, as occurs during positive PDO phases, contributes decadal periods of high flows and vice versa for negative PDO phases. In particular the declining flow over recent decades can be explained in terms of decadal changes in Pacific and Atlantic SSTs toward a state (cold tropical Pacific – warm tropical North Atlantic) that is ideal for inducing dry conditions over the URG headwaters. As Rio Grande flow will be impacted by human driven climate change this information on natural variation of flow is essential for its management, lying as it does in a region where climate models project an increasingly arid climate (Seager et al., 2007; Vano et al., 2014; Ault et al., 2014).

Conflict of interest

The authors declare that they have no conflict of interest.

Acknowledgements

References

Adams, D.K., Comrie, A.C., 1997. The North American Monsoon. Bull. Am. Meteorol. Soc. 78 (10), 2197–2213. http://dx.doi.org/10.1175/1520-0477(1997) 078<2197:TNAM>2.0.CO;2.

Ault, T.R., Cole, J.E., Overpeck, J.T., Pederson, G.T., Meko, D.M., 2014. Assessing the risk of persistent drought using climate model simulations and paleoclimate data. J. Climate 27 (20), 7529–7549.

Barlow, M., Nigam, S., Berbery, E., 1998. Evolution of the North American Monsoon system. J. Climate 11 (9), 2238–2257. http://dx.doi.org/10.1175/1520-0442(1998)011<2238:EOTNAM>2.0.CO;2.

Barlow, M., Nigam, S., Berbery, E.H., 2001. ENSO, Pacific decadal variability, and U.S. summertime precipitation, drought, and stream flow. J. Climate 14 (9), 2105–2128. http://dx.doi.org/10.1175/1520-0442(2001)014<2105:EPDVAU>2.0.CO;2.

Córdoba-Machado, S., Palomino-Lemus, R., Gámiz-Fortis, S.R., Castro-Díez, Y., Esteban-Parra, M.J., 2016. Seasonal streamflow prediction in Colombia using atmospheric and oceanic patterns. J. Hydrol. 538, 1–12.

Cayan, D., Redmond, K., Riddle, L., 1999. ENSO and hydrologic extremes in the western United States (vol. 12, pg. 2881, 1999). J. Climate 12 (12), 3516.

Chen, X., Wallace, J.M., 2015. ENSO-like variability: 1900–2013. J. Climate 28 (24), 9623–9641. http://dx.doi.org/10.1175/JCLI-D-15-0322.1.

Cook, B.I., Seager, R., Miller, R.L., 2011. On the causes and dynamics of the early twentieth-century North American pluvial. J. Climate 24 (19), 5043–5060. http://dx.doi.org/10.1175/2011JCLI4201.1.

Daly, C., Halbleib, M., Smith, J.I., Gibson, W.P., Doggett, M.K., 2008. Physiographically sensitive mapping of climatological temperature and precipitation across the conterminous United States. Int. J. Climatol. 28 (15), 2031–2064. http://dx.doi.org/10.1002/joc.1688.

Dee, D.P., Uppala, S.M., Simmons, A.J., Berrisford, P., Poli, P., Kobayashi, S., Andrae, U., Balmaseda, M.A., Balsamo, G., Bauer, P., Bechtold, P., Beljaars, A.C.M., van de Berg, L., Bidlot, J., Bormann, N., Delsol, C., Dragani, R., Fuentes, M., Geer, A.J., Haimberger, L., Healy, S.B., Hersbach, H., Hólm, E.V., Isaksen, L., Kållberg, P., Köhler, M., Matricardi, M., McNally, A.P., Monge-Sanz, B.M., Morcrette, J.-J., Park, B.-K., Peubey, C., de Rosnay, P., Tavolato, C., Thépaut, J.-N., Vitart, F., 2011. The ERA-Interim reanalysis: configuration and performance of the data assimilation system. Q. J. R. Meteorol. Soc. 137 (656), 553–597. http://dx.doi.org/10.1002/qj.828.

Enfield, D.B., Mestas-Nunez, A., Trimble, P., 2001. The Atlantic multidecadal oscillation and its relation to rainfall and river flows in the continental U.S. Geophys. Res. Lett. 28 (10), 2077–2080.

Guan, H., Vivoni, E.R., Wilson, J.L., 2005. Effects of atmospheric teleconnections on seasonal precipitation in mountainous regions of the southwestern US: a case study in northern New Mexico. Geophys. Res. Lett. 32 (23).

Hamlet, A.F., Mote, P.W., Clark, M.P., Lettenmaier, D.P., 2007. Twentieth-century trends in runoff, evapotranspiration, and soil moisture in the western united states. J. Climate 20 (8), 1468–1486. http://dx.doi.org/10.1175/JCLI4051.1.

Kahya, E., Dracup, J.A., 1993. US streamflow patterns in relation to the El Niño/Southern Oscillation. Water Resour. Res. 29 (8), 2491–2503.

Kahya, E., Dracup, J.A., 1994. The influences of type 1 El Nino and La Nina events on streamflows in the Pacific southwest of the United States. J. Climate 7 (6), 965–976.

Khedun, C., Mishra, A., Özger, M., Kato-Beaudoing, H., Bolten, J., Giardino, J., Singh, V., 2010. Assessing the impacts of climate variability on the water resources in the Rio Grande/Río Bravo basin. Am. Soc. Civil Eng. 69–80. http://dx.doi.org/10.1061/41114(371)9.

Kiem, A.S., Franks, S.W., 2004. Multi-decadal variability of drought risk, eastern Australia. Hydrol. Process. 18 (11), 2039–2050.

Kiem, A.S., Franks, S.W., Kuczera, G., 2003. Multi-decadal variability of flood risk. Geophys. Res. Lett. 30 (2), 1035. http://dx.doi.org/10.1029/2002GL015992.

King, A.D., Alexander, L.V., Donat, M.G., 2013. The efficacy of using gridded data to examine extreme rainfall characteristics: a case study for Australia. Int. J. Climatol. 33 (10), 2376–2387. http://dx.doi.org/10.1002/joc.3588.

Koster, R.D., Mahanama, S.P.P., Livneh, B., Lettenmaier, D.P., Reichle, R.H., 2010. Skill in streamflow forecasts derived from large-scale estimates of soil moisture and snow. Nat. Geosci. 3 (9), 613–616. http://dx.doi.org/10.1038/ngeo944.

Kushnir, Y., Seager, R., Ting, M., Naik, N., Nakamura, J., 2010. Mechanisms of tropical Atlantic SST influence on North American precipitation variability. J. Climate 23 (21), 5610–5628. http://dx.doi.org/10.1175/2010JCLI3172.1.

Lee, S., Klein, A., Over, T., 2004. Effects of the El Niño-Southern oscillation on temperature, precipitation, snow water equivalent and resulting streamflow in the Upper Rio Grande river basin. Hydrol. Process. 18 (6), 1053–1071. http://dx.doi.org/10.1002/hyp.5511.

Llewellyn, D., Vaddey, S., 2013. West-wide Climate Risk Assessment: Upper Rio Grande Impact Assessment: Report. US Department of the Interior, Bureau of Reclamation, Upper Colorado Region, Albuquerque Area Office.

Maurer, E.P., Lettenmaier, D.P., 2003. Predictability of seasonal runoff in the Mississippi River basin. J. Geophys. Res.: Atmos. 108 (D16), 8607. http://dx.doi.org/10.1029/2002JD002555.

McCabe, G., Palecki, M., Betancourt, J., 2004. Pacific and Atlantic Ocean influences on multidecadal drought frequency in the United States. Proc. Natl. Acad. Sci. 101 (12), 4136–4141. http://dx.doi.org/10.1073/pnas.0306738101.

Nowak, K., Hoerling, M., Rajagopalan, B., Zagona, E., 2012. Colorado River basin hydroclimatic variability. J. Climate 25 (12), 4389–4403. http://dx.doi.org/10.1175/JCLI-D-11-00406.1.

Pascolini-Campbell, M.A., Seager, R., Gutzler, D.S., Cook, B.I., Griffin, D., 2015. Causes of interannual to decadal variability of Gila River streamflow over the past century. J. Hydrol.: Reg. Stud. 3, 494–508. http://dx.doi.org/10.1016/j.ejrh.2015.02.013. http://www.sciencedirect.com/science/article/pii/S2214581815000178.

Schubert, S., 2009. A U.S. CLIVAR project to assess and compare the responses of global climate models to drought-related SST forcing patterns: overview and results. J. Climate 22 (19), 5251–5272. http://dx.doi.org/10.1175/2009JCLI3060.1.

Seager, R., Ting, M., Held, I., Kushnir, Y., Lu, J., 2007. Model projections of an imminent transition to a more arid climate in southwestern North America. Science 316 (5828), 1181–1184. http://dx.doi.org/10.1126/science.1139601.

Smith, T.M., Reynolds, R.W., Peterson, T.C., Lawrimore, J., 2008. Improvements to NOAA's historical merged land-ocean surface temperature analysis (1880–2006). J. Climate 21 (10), 2283–2296. http://dx.doi.org/10.1175/2007JCLI2100.1.

Thomas, B.E., 2007. Climatic fluctuations and forecasting of streamflow in the lower Colorado River basin. J. Am. Water Resour. Assoc. 43 (6), 1550–1569.

Tozer, C.R., Kiem, A.S., Verdon-Kidd, D.C., 2012. On the uncertainties associated with using gridded rainfall data as a proxy for observed. Hydrol. Earth Syst. Sci. 16 (5), 1481–1499. http://dx.doi.org/10.5194/hess-16-1481-2012. http://www.hydrol-earth-syst-sci.net/16/1481/2012/.

Trenberth, K.E., Branstator, G.W., Karoly, D., Kumar, A., Lau, N.-C., Ropelewski, C., 1998. Progress during TOGA in understanding and modeling global tele-connections associated with tropical sea surface temperatures. J. Geophys. Res.: Oceans 103 (C7), 14291–14324. http://dx.doi.org/10.1029/97JC01444.

Vano, J.A., Udall, B., Cayan, D.R., Overpeck, J.T., Brekke, L.D., Das, T., Hartmann, H.C., Hidalgo, H.G., Hoerling, M., McCabe, G.J., et al., 2014. Understanding uncertainties in future Colorado River streamflow. Bull. Am. Meteorol. Soc. 95 (1), 59–78.

Ward, P.J., Kummu, M., Lall, U., 2016. Flood frequencies and durations and their response to El Niño Southern oscillation: global analysis. J. Hydrol. 539, 358–378. http://dx.doi.org/10.1016/j.jhydrol.2016.05.045. http://www.sciencedirect.com/science/article/pii/S0022169416303122.

Woodhouse, C.A., Kunkel, K.E., Easterling, D.R., Cook, E.R., 2005. The twentieth-century pluvial in the western United States. Geophys. Res. Lett. 32 (7). http://dx.doi.org/10.1029/2005GL022413.

Woodhouse, C.A., Stahle, D.W., Villanueva Diaz, J., 2012. Rio Grande and Rio Conchos water supply variability over the past 500 years. Climate Res. 51 (2), 147.

Zhang, Y., Wallace, J.M., Battisti, D.S., 1997. ENSO-like interdecadal variability: 1900–93. J. Climate 10 (5), 1004–1020. http://dx.doi.org/10.1175/1520-0442(1997)010<1004:ELIV>2.0.CO;2.